ISIJ International, Vol. 45 (2005), No. 6, pp. 876–885

Prediction of Acicular Ferrite from Flux Ingredients in Submerged Arc Weld Metal of C–Mn Steel

Prasanta KANJILAL, Sujit Kumar MAJUMDAR[1)] and Tapan Kumar PAL[2)]

Mechanical Engg. Divn., National Test House, Salt Lake, Kolkata-700 091, India. E-mail: dgnth@wb.nic.in
1) SQC & OR Dept., Indian Statistical Institute, Kolkata-700 035, India. E-mail: skm@isical.ac.in
2) Metallurgical Engg. Dept., Jadavpur University, Kolkata-700 032, India. E-mail: t_k_pal@yahoo.com

(*Received on July 29, 2004; accepted on April 7, 2005*)

The prediction model has been developed for low carbon steel weld metal acicular ferrite microstructure as a function of flux ingredients such as CaO, MgO, CaF_2 and Al_2O_3 in submerged arc welding carried out at fixed welding parameters. The results of quantitative measurements of acicular ferrite (AF) on eighteen no. of weld metal samples were utilised for developing the prediction model. Among the flux ingredients, CaO appears to be most important as an individual as well as interaction with other ingredients in controlling the amount of acicular ferrite content in the weld metal. Furthermore, formation of acicular ferrite is also related to the weld bead geometry which is influenced by flux ingredients. The prediction equation for acicular ferrite has been checked for adequacy by performing separate experiments on welding using randomly designed flux. The isoresponse curves were developed to show the level of acicular ferrite content at different percentage of flux ingredients.

KEY WORDS: submerged arc welding; statiscal experiment for mixture; extreme vertices design; flux ingredients; synergism; antagonism; carbon equivalent; inclusion characteristics; weld bead parameter.

1. Introduction

Weldment properties are influenced by its macro and microstructures. In submerged arc welding, microstructure of as-deposited weld metal depends upon the chemical composition of the steel base plate and filler metal, the composition of the flux used during welding and the cooling rate of the weld metal during transformation of undercooled metastable austenite. Several different microstructures can be obtained in the weld metal of C–Mn steel. They are grain boundary ferrite, side plate ferrite, polygonal ferrite, acicular ferrite, ferrite with aligned second phase or upper bainite.[1)] Along with them lower bainite and martensite are also observed in small amount.[2)]

It has been recognized that increasing amount of acicular ferrite provides both increased toughness and improved strength in low carbon steel weld metals.[3–5)] Therefore several studies have been made to understand the mechanism of the acicular ferrite formation in weld metal. Factors such as alloy hardenability, austenite grain size and weld cooling rate play a very important role in determining whether or not acicular ferrite will form. However, recent investigations have suggested[5–9)] that oxygen affects the weld metal microstructure in the form of inclusions. Lower levels of total oxygen ($<$200 ppm) mean that insufficient inclusion numbers are generated for the formation of acicular ferrite so that other microconstituents such as bainite or widmanstaten ferrite are formed preferentially. Increasing total oxygen content much above 300 ppm apparently generates many more small oxide inclusions ($<0.2\,\mu$m) which can pin austenite grain boundaries and reduce prior austenite grain size so that grain boundary-nucleated microconstituents form rather than acicular ferrite.[10–12)] For example, Dallam *et al.*[13)] obtained 90% acicular ferrite in submerged arc HSLA weld metal using CaF_2–CaO–SiO_2 flux system with corresponding oxygen content from 200–300 ppm. These inclusions usually contain manganese, silicon, aluminium and titanium as their major constituents. The experimental results and the calculations of Babu *et al.*[14)] strongly suggest that composition of inclusion will depend on the weld metal composition, particularly with respect to the major deoxidizing elements, Mn, Si, Al and Ti and the welding conditions.

In the SAW process the main source of weld metal oxygen is the flux.[15,16)] The behaviour of flux as characterized in terms of basicity index could be considered as rough guide,[17)] since it has failed to address the fundamental question of transfer of oxygen from flux to weld as well as the extent of slag metal reactions in the weld pool.[18,19)] Later oxygen potential has been considered to facilitate better prediction of flux behaviour.[18–20)] However, stability of flux ingredients based on free energy of formation has been shown to be altered in the presence of welding plasma.[21)]As such element transfer from the slag to weld metal and *vice versa* may not be accurately predicted based on thermodynamic data.[22)] Furthermore, physical properties of flux such as viscosity, thermal conductivity, fluidity *etc*. have also been observed to have significant effect on weld metal chemistry.[23)]

It becomes clear that acicular ferrite formation is a com-

plex phenomenon with multiple factors and mechanisms operating simultaneously. The target structure and properties are commonly obtained by adjusting variables such as current, voltage, speed and wire-flux combination by trial and error. Since flux plays an important role in the final weld metal composition and inclusion characteristics in SAW process, understanding the flux composition and microstructure of the weld metal remains a major objective in producing maximum amount of acicular ferrite and thereby optimum mechanical properties.

The aim of the present work is to predict acicular ferrite content of the microstructure of weld metal, made with different flux ingredients in CaO–MgO–CaF_2–Al_2O_3 flux system using given filler wire and welding parameters in order to provide a rational basis for choosing flux composition. This is important in order to establish flux formulation for optimum mechanical properties.

2. Planning of the Experiments

The Idea of this present set of investigations is to take account simultaneous variation of each flux ingredient in a flux mixture in order to find out the effect of each flux ingredient as well as their interaction effects on weld metal microstructural constituent acicular ferrite. This has been made possible by applying "statistical design of experiment" involving mixtures, in particular "extreme vertices design", according to which proportions of the important flux ingredients were varied simultaneously to investigate the simultaneous effect of each flux ingredient and their interactions on weld metal microstructure in CaO–MgO–CaF_2–Al_2O_3 flux system.

• Extreme Vertices Design Algorithm

In experiments using mixture of q components, the components are expressed as a fraction x of the total mixture and the response is a function of the proportions of the components and not the total amount of mixture. The extreme vertices design that was used for experimentation[24–26] consisted of the 10 admissible vertices of the polyhedron, 7 centroids of the seven two-dimensional faces and the overall centried. Thus although 10 coefficients of the quadratic regression model (as shown in Eq. (1)) for the response characteristics were required to be estimated, 18 design points were deliberately chosen for getting better estimates of the coefficients and error. The above design was obtained by following the two step procedures of Mclean and Anderson.[25] After having generated $4\times2^{4-1}=32$ possible combinations of the four components, it was bound that there was 10 admissible vertices which satisfied the constraint for the mixture total as also the lower and upper bounds of each component proportion. The seven two-dimensional faces of the polyhedron were found by grouping the vertices of the polyhedron into groups of 3 or more vertices where each vertex had the same value x_i for one of the four components. Thus, the coordinates of the seven two-dimensional faces which satisfied the constraints are the design points sl. 11 to 17. The design point sl. no. 18 was the overall centroid which was the average of all the 10 vertices. The trace $(x'x)^{-1}$, where x represents the complete design matrix of the given design was also small. In 3D space the constraint design regent is shown in the **Fig. 1** which represents the mixture space in the present experiment.

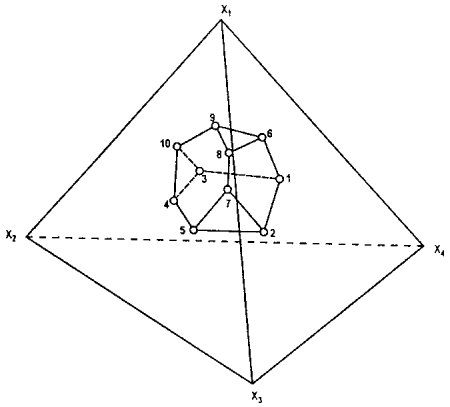

Fig. 1. The constrained factor space inside the tetrahedron describing the experimental space.

Snee[27] also gave the algorithm for selecting the subsets of extreme vertices for fitting quadratic models of the following form in the constrained mixture spaces.

$$y=\sum_{i=1}^{q}\beta_i x_i+\sum_{i<j}^{q}\sum^{q}\beta_{ij}x_i x_j \quad \text{.....(1)}$$

The regression coefficients β_i and β_{ij} are the least square estimates in the fitted model and y is the response variable.

The percentage variation of a given response characteristic is measured by the term 'R^2', which is evaluated from the relation

$$R^2=1-\frac{\text{SSE}}{\text{SST}} \quad \text{.....(2)}$$

SSE: sun of square of errors

SST: total sum of square

In the present experiment flux ingredient (x_i) has four constituents *viz.*, x_1=CaO, x_2=MgO, x_3=CaF_2 and x_4=Al_2O_3.

3. Experimental Procedure

3.1. Preparation of Agglomerated Flux

Eighteen no. of agglomerated fluxes used in the study were prepared by varying the ingredients CaO, MgO, CaF_2 and Al_2O_3 as per formulations based on statistical mixture design are given in **Table 1**. The flux ingredients such as CaO, MgO, CaF_2, Al_2O_3 SiO_2, Fe–Mn, Fe–Si and nickel powder of size 70–230 mm were first weighed separately as per their weight percentage in a spring balance (±0.02 g) and initially mixed manually within a container. Then the dry mixture was taken in a rotating mixer m/c and operated for 3 h. It was then transferred to the agglomerating machine and mixed with silicate binder for 1 h. The agglomerated mass were allowed to dry in air for 24 h. Then it was taken in a stainless steel container and heated in a furnace at a temperature of 700°C for 1 h duration to remove moisture and other volatile matter. Thereafter it was taken from the furnace and cooled in air. The size classification of the agglomerated mass was done by shieve shaker.

Table 1. Design matrix of flux used in submerged arc welding.

Sample No.	Mixture Variables Composition			
	CaO (wt%)	MgO (wt%)	CaF_2 (wt%)	Al_2O_3 (wt%)
P1	15.00	15.00	10.00	40.00
P2	15.00	15.00	40.00	10.00
P3	15.00	32.40	10.00	22.60
P4	15.00	17.00	40.00	8.00
P5	15.00	32.40	24.60	8.00
P6	35.00	15.00	10.00	20.00
P7	17.00	15.00	40.00	8.00
P8	35.00	15.00	22.00	8.00
P9	29.60	32.40	10.00	8.00
P10	35.00	27.00	10.00	8.00
P11	24.43	23.14	24.43	8.00
P12	15.67	15.67	40.00	8.66
P13	25.92	24.36	10.0	19.72
P14	23.40	15.00	24.40	17.20
P15	19.87	32.40	14.86	12.87
P16	15.00	22.36	24.92	17.72
P17	35.00	19.00	14.00	12.00
P18	22.67	21.63	21.63	14.07

Other Additions to eighteen nos. of flux samples
Wt% SiO_2 = 10.0 Wt% Fe-Mn = 4.0
Wt% Bentonite = 2.0 Wt% Fe-Si = 3.0
Wt% Ni-Powder = 1.0

3.2. Submerged Arc Welding

Low carbon steel plates of dimensions 100 mm×250 mm×18 mm were used as base plate. Welding was performed with an automatic submerged arc welding machine with constant voltage power supply rectifier, welding current being controlled by the wire feed rate. Before welding, fluxes were dried at a temperature of 300°C for 3 h in an oven. Single pass bead-on-plate weld deposits were made on 18 mm thick base plate using 3.15 mm dia AWS type A 5.17 EL8 mild steel filler wire and agglomerated submerged arc fluxes as given in Table 1. Direct current reverse polarity with constant current of 400 A., voltage 26 V, horizontal travel speed of 4.65 mm/s. and electrode extension of 25 mm wire maintained during welding of eighteen no. of samples.

3.3. Chemical Composition Analysis

Chemical constituents such as carbon, manganese, silicon, sulphur, phosphorous and nickel of the base metal, filler wire and weld metal were analysed by Quantovoc method. Oxygen and nitrogen contents were measured by Leco interstitial analyzer. Cylindrical samples of 3 mm dia and 9 mm length prepared by machining were used for this purpose. The chemical composition of filler wire, base metal and weld metal are given separately in **Table 2**.

3.4. Microscopic Examination

Each of the eighteen no. of samples were cut transverse to the weld direction and prepared for microscopic studies on weld metal zone. Samples were examined first under optical microscope and various micro-structural constituents were identified. The quantitative measurement of the microstructural constituents were performed by conventional two dimensional Point Counting method using ELECO automatic point counter. The results are given in **Table 3**. The weld metal samples were also examined under optical microscope to find out volume fraction and size distribution of inclusions as per previous investigation.[28,29] Few selected samples were examined under Transmission electron microscope. TEM micrographs were taken for selected samples. In order to study the weld metal inclusion composition, EDAX method in Scanning Electron Microscope (JEOL JASM 840 A operated at 20 kV) was used.

4. Results

4.1. Prediction Equation for Weld Metal Microstructural Constituents

Since all welding are carried out at constant weld parameters, the wide variations of microstructural constituents in weld metal samples given in Table 3 reflects the effects of flux ingredients on the formation of weld metal microstructural constituents.

The experimentally determined values of weld metal acicular content (Table 3) were used to develop prediction equation for the response acicular ferrite (AF). Adequate quadratic regression model in canonical form was developed for acicular ferrite (AF) content as functions of wt% of flux ingredients (CaO, MgO, CaF_2 and Al_2O_3) using the module of constrained mixture design of statistica. The prediction equation for acicular ferrite is given below:

$$\begin{aligned}\text{Acicular Ferrite (AF\%)} = & -4.8335\text{CaO}+2.0808\text{MgO} \\ & -0.3680\text{CaF}_2-0.6867\text{Al}_2\text{O}_3 \\ & +0.0756\text{CaO}\cdot\text{MgO} \\ & +0.1551\ \text{CaO}\cdot\text{CaF}_2 \\ & +0.1701\text{CaO}\cdot\text{Al}_2\text{O}_3 \\ & -0.0731\text{MgO}\cdot\text{CaF}_2 \\ & -0.0721\text{MgO}\cdot\text{Al}_2\text{O}_3 \\ & -0.0068\text{CaF}_2\cdot\text{Al}_2\text{O}_3 \end{aligned} \quad \text{.....(3)}$$

The details of regression model are given in Appendix I.

4.2. Nature of Variation of Microstructural Constituents with the Flux Ingredients and Their Binary Mixtures

It is observed from the above prediction results (Eq. (3)) that flux ingredients have two types of effect on weld metal acicular ferrite contents, *viz.* (i) Individual effect and (ii) Interaction effect of binary mixture. It is to be noted from the prediction equation of acicular ferrite that only "statistically significant" variables and/or their binary synergism/antagonism will be considered to have predominant effect on the given response characteristics. In the developed prediction equation for acicular ferrite, (Eq. (3)) only those individual flux ingredients (x_i) and their binary mixture (x_ix_j) are considered significant, when their p-value (significant level) are nearly equal to 0.05 (equivalent to 95% confidence level) as given in Appendix I. The other non-significant variables, although constitute a part of the prediction equations, can not be considered to have predominant effect on the response, because these effects are not distinguishable from the random noise generated in the experiments. The predominant effects of flux ingredients and their binary mixtures on weld metal micro structural constituent acicular ferrite are summarised in **Table 4.**

Table 2. Chemical compositions of base metal, filler wire and eighteen no. of weld metal samples (P1–P18).

Sample No.	Carbon (wt%)	Manganese (wt%)	Silicon (wt%)	Sulphur (wt%)	Phosphorous (wt%)	Nickel (wt%)	Oxygen (ppm)	Nitrogen (ppm)
Base Metal	0.22	0.77	0.25	0.03	0.02	Nil	350	50
Filler Wire	0.10	0.56	0.05	0.02	0.01	Nil	380	60
Weld Metal Samples								
No. P1	0.070	0.560	0.340	0.042	0.025	0.21	560	92
" P2	0.070	0.520	0.210	0.042	0.028	0.11	570	95
" P3	0.070	0.620	0.280	0.040	0.025	0.20	520	103
" P4	0.060	0.470	0.170	0.034	0.023	0.17	500	86
" P5	0.068	0.600	0.248	0.044	0.024	0.27	530	86
" P6	0.098	0.670	0.229	0.028	0.021	0.24	380	36
" P7	0.072	0.488	0.270	0.040	0.026	0.32	490	38
" P8	0.070	0.580	0.200	0.028	0.022	0.29	480	22
" P9	0.068	0.690	0.260	0.027	0.023	0.23	330	31
" P10	0.063	0.540	0.193	0.034	0.022	0.31	480	39
" P11	0.073	0.700	0.120	0.021	0.050	0.50	300	32
" P12	0.095	0.601	0.150	0.037	0.070	0.34	350	43
" P13	0.084	0.620	0.160	0.016	0.032	0.30	320	52
" P14	0.089	0.748	0.258	0.031	0.077	0.78	300	36
" P15	0.094	0.800	0.370	0.020	0.046	0.59	320	38
" P16	0.061	0.507	0.200	0.024	0.025	0.05	600	76
" P17	0.082	0.595	0.273	0.015	0.045	0.33	470	45
" P18	0.058	0.517	0.160	0.023	0.052	0.29	540	101

Table 3. Microstructure content of eighteen no. of weld metal samples.

Sample No.	Microstructure %				
	GBF	SPF	PF	AF	FAS
P1	37	19	27	13	4
P2	38	19	27	12	4
P3	31	18	30	15	6
P4	34	17	30	14	5
P5	38	17	27	13	5
P6	29	16	24	24	7
P7	34	20	25	16	5
P8	31	16	29	19	5
P9	29	17	20	28	6
P10	31	19	29	16	5
P11	24	14	20	35	7
P12	29	15	24	26	6
P13	27	12	27	28	6
P14	22	10	25	36	7
P15	25	14	18	35	8
P16	34	21	31	10	4
P17	32	14	28	20	6
P18	33	19	28	16	4

GBF = Grain Boundary Ferrite
SPF = Side Plate Ferrite
PF = Polygonal Ferrite
AF = Acicular Ferrite
FAS = Ferrite with aligned second phase (Upper bainite)

Table 4. Predominant effect of flux ingredients and their binary mixtures on acicular ferrite and weld bead parameters (s/a).

(Response characteristics)	Predominant Effects			
	Pure flux Ingredient		Binary Mixtures of Flux Ingredient	
	Increase	Decrease	Synergism	Antagonism
a) **Microstructural constituents** Acicular ferrite (AF)	—	CaO	$CaO\text{-}CaF_2$, $CaO\text{-}Al_2O_3$	—
b) Inclusion volume fraction (V_f)	CaF_2	—	—	—
c) Inclusion no. density (D_o)	—	—	CaO-MgO $MgO\text{-}CaF_2$ $MgO\text{-}Al_2O_3$ $CaF_2\text{-}Al_2O_3$	—
d) Weld Bead parameter (S/A)	CaO, CaF_2, Al_2O_3	—	—	$CaO\text{-}CaF_2$, $CaO\text{-}Al_2O_3$

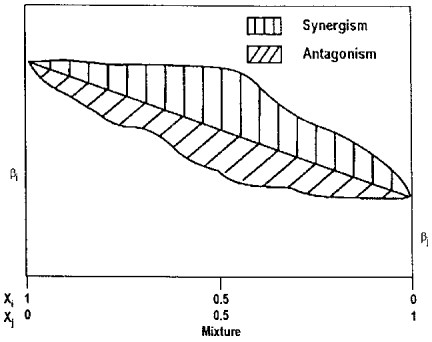

Fig. 2. Synergism and antagonism of binary mixtures.

The concept of binary synergism and antagonism is quite different from the individual effect. The binary synergism/antagonism implies that the response (weld metal acicular ferrite content) obtained due to binary mixture is more than/less than the average of that response produced by two pure flux ingredients forming the same binary mixture. This is shown schematically in **Fig. 2**. The positive and negative sign of the coefficients β_i in Eq. (1) indicates increase or decrease of that response variable (y) by the flux ingredients (x_i) respectively. Similarly either positive or negative sign of coefficients β_{ij} in the Eq. (1), indicates binary synergistic or antagonistic effect of the flux mixture ($x_i x_j$) on the response variable.

5. Discussion

The summarized results of the predominant effects of flux ingredients and their binary mixtures on acicular ferrite (Table 4) show that flux ingredient CaO decreases weld metal acicular ferrite (AF) content. However, flux mixtures $CaO\text{–}CaF_2$ and $CaO\text{–}Al_2O_3$ have binary synergistic (increasing) effect on weld metal acicular ferrite (AF) content. Acicular ferrite content in the present study varies from

(a) Sample P2

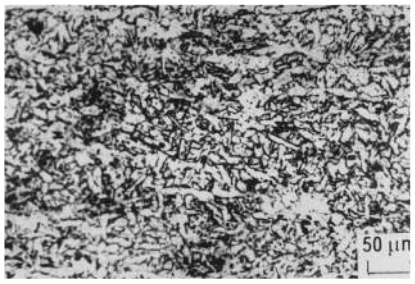

(b) Sample P14

Fig. 3. Optical micrograph of weld metal samples, (a) P2 containing 12% acicular ferrite, (b) P14 containing 36% acicular ferrite.

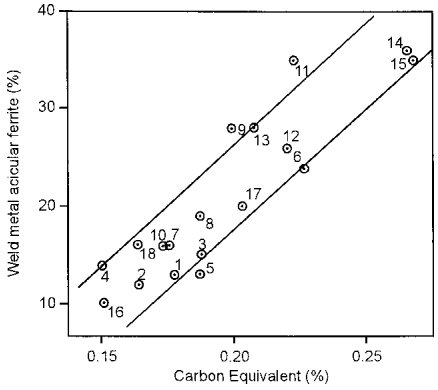

Fig. 4. Effect of carbon equivalent (CE) on weld mental acicular ferrite content for different samples.

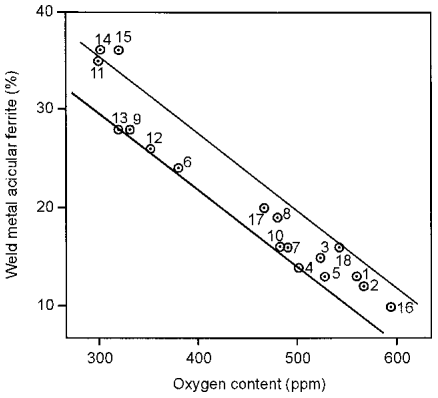

Fig. 5. Effect of oxygen content on weld metal acicular ferrite content for different samples.

Table 5. Inclusion volume fraction and number density of weld metal samples.

Sample No.	Volume Fraction, (V_f)	Density (n_o/mm^2)
P1	5.0×10^{-3}	5.95×10^{4}
P2	5.4×10^{-3}	5.90×10^{4}
P3	4.3×10^{-3}	5.60×10^{4}
P4	4.2×10^{-3}	5.51×10^{4}
P5	5.2×10^{-3}	6.05×10^{4}
P6	3.8×10^{-3}	4.95×10^{4}
P7	4.6×10^{-3}	6.00×10^{4}
P8	4.2×10^{-3}	4.80×10^{4}
P9	3.5×10^{-3}	4.62×10^{4}
P10	4.8×10^{-3}	5.35×10^{4}
P11	2.9×10^{-3}	3.75×10^{4}
P12	3.9×10^{-3}	4.80×10^{4}
P13	3.5×10^{-3}	4.50×10^{4}
P14	3.0×10^{-3}	3.70×10^{4}
P15	3.2×10^{-3}	3.75×10^{4}
P16	4.8×10^{-3}	5.80×10^{4}
P17	4.4×10^{-3}	5.50×10^{4}
P18	4.6×10^{-3}	5.20×10^{4}

12% in sample P2 (**Fig. 3**(a)) to 36% in sample P14 (Fig. 3(b)). It has been well established that the weld metal chemical composition has direct influence over AF formation.[30–32] The elements such as carbon, manganese and nickel increase the hardenability and move austenite transformation start curves to longer times and increases the AF formation. On the other hand, sulphur and oxygen move the transformation curves to shorter times and therefore decreases the AF content. It is pertinent to mention here that the prediction equations for weld metal chemical constituents were also developed by the authors in terms of wt% of flux ingredients using the same design of experiment in their previous work.[33] The details of prediction equations along with the predominant effect of each flux ingredients and their binary mixtures on weld metal Oxygen, Manganese, Silicon, Sulphur, Carbon and Nickel content were summarized in Appendix II.

Considering the prediction results of AF as given in Table 4, flux ingredient CaO may be expected to reduce weld metal AF content since CaO also increases weld metal oxygen content.[33] The binary synergistic (increasing) effect of CaO–CaF_2 and CaO–Al_2O_3 mixture on AF could be attributed due to (i) Binary synergistic (increasing) effect of CaO–CaF_2 mixture on Mn and Ni content, (ii) Binary synergistic (increasing) effect of CaO–Al_2O_3 mixture on C, Mn and Ni content and (iii) Binary antagonistic (decreasing) effect of both CaO–CaF_2 and CaO-Al_2O_3 mixtures on oxygen content,[33] which are also detailed in Appendix II.

Since AF formation is dependent on hardenability elements and oxygen content, the percentage of weld metal AF has been plotted with elements in terms of carbon equivalent[34] and oxygen content as given in **Figs. 4** and **5** respectively. Considerable scatter depicted in Figs. 4 and 5 probably indicate some other factors involved with AF formation in addition to CE and oxygen content. These could be due to the inclusions *e.g.* inclusion volume fraction, size, composition and intragranular inclusion density in weld metal, as reported by several authors.[35,36] With increase in inclusion volume fraction and inclusion density, (**Table 5**), weld metal AF content is found to decrease as shown in **Figs. 6** and **7**. However, wide variation of AF content still persists even at a fixed inclusion volume fraction and density, indicating other factor such as inclusion size, intragranular density and composition which are also operative in controlling AF. Considering the importance of inclusion in AF formation, prediction models were also developed like AF for inclusion volume fraction (V_f) and no. density (D_o) of weld metal samples in terms of flux ingredients and their binary mixture as given in Eqs. (4) and (5) respectively.

$$\begin{aligned} V_f = {} & 0.4804\mathrm{CaO} + 0.7807\mathrm{MgO} + 0.0274\mathrm{CaF_2} \\ & + 0.6188\mathrm{Al_2O_3} + 0.0360\mathrm{CaO \cdot MgO} \\ & + 0.0203\mathrm{CaO \cdot CaF_2} + 0.0299\mathrm{CaO \cdot Al_2O_3} \\ & + 0.0118\mathrm{MgO \cdot CaF_2} + 0.0102\mathrm{MgO \cdot Al_2O_3} \\ & + 0.0266\mathrm{CaF_2 \cdot Al_2O_3} \quad \ldots\ldots (4) \end{aligned}$$

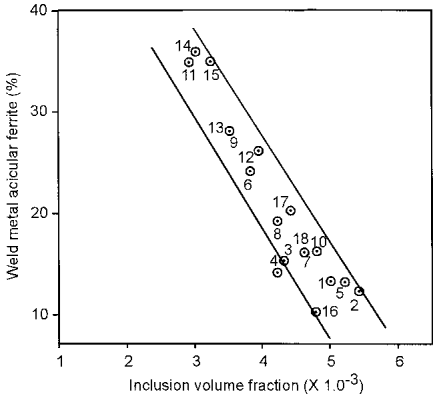

Fig. 6. Variation of weld metal acicular ferrite content with inclusion volume fraction for different samples.

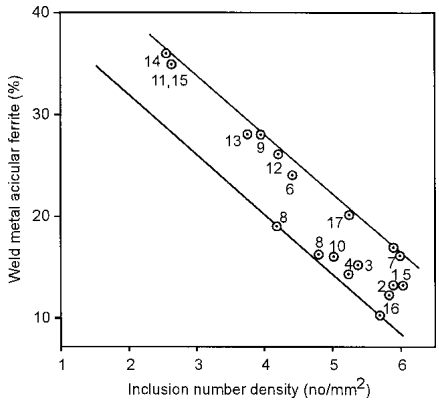

Fig. 7. Variation of weld metal acicular ferrite content with inclusion number density for different samples.

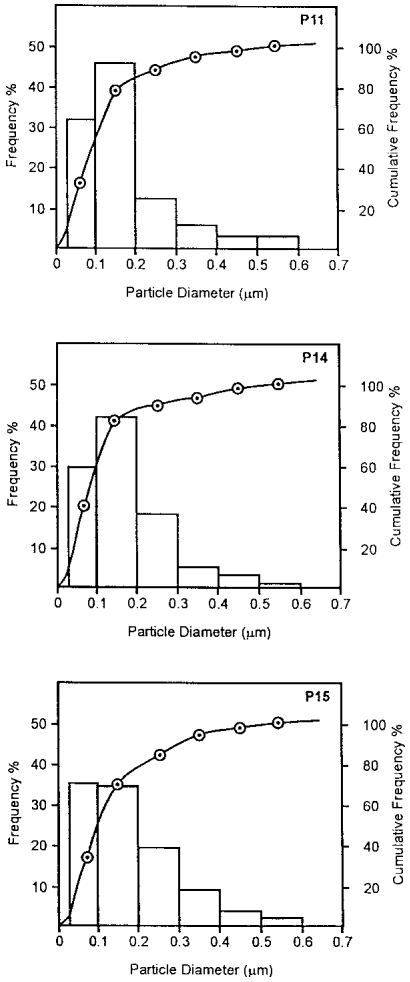

Fig. 8. Simple and cumulative size distribution of the inclusions extracted from weld metal samples (a) P11, (b) P14 and (c) P15.

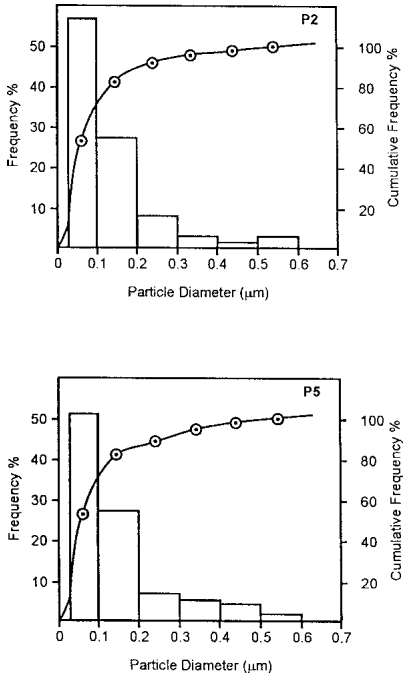

Fig. 9. Simple and cumulative size distribution of the inclusions extracted fro weld metal samples (a) P2 and (b) P5.

$$D_o = 0.1123CaO - 0.8307MgO + 0.3120CaF_2 + 0.2076Al_2O_3 + 0.0778CaO \cdot MgO + 0.0346CaO \cdot CaF_2 + 0.0315CaO \cdot Al_2O_3 + 0.0552MgO \cdot CaF_2 + 0.0547MgO \cdot Al_2O_3 + 0.0431CaF_2 \cdot Al_2O_3 \quad \ldots\ldots(5)$$

The predominant effect of flux ingredients and their binary mixtures on V_f and D_o are summarized in Table 4. The details of regression models are also given in Appendix I. The results (Table 4) show that flux ingredient CaF_2 increases inclusion volume fraction and this will increase the grain boundary area favouring grain boundary ferrite only.[28] Therefore, CaF_2 may be expected to increase the microstructural constituent GBF.

On the other hand, the binary mixture of CaO–MgO, MgO–CaF_2, MgO–Al_2O_3 and CaF_2–Al_2O_3 show binary synergistic (increasing) effect on inclusion number density (Eq. (5) and Table 4). With the increase of inclusion number density, more no. of inclusions are available at grain boundary region, thus favouring high temperature transformation products like GBF, SPF. Therefore, it can be stated that flux mixtures *viz*. (CaO–MgO, MgO–CaF_2, MgO–Al_2O_3 and CaF_2–Al_2O_3) have no supporting role in AF formation. This is also reflected in the prediction results of AF (Table 4) where these flux mixtures are shown to have no significant effect on AF formation.

Several investigators[29,35,36] have reported that maximum AF (~80%) is associated with average inclusion size of 0.35 μm, optimum intragranular density of 0.5×10^8 no./mm^2. In the present set of experiments, the sample P14 and P15 having lower inclusion density (~3.75×10^4 no./mm^2) and coarser average inclusion size (0.266 μm and 0.226 μm respectively) show higher amount of AF (36%) as compared to sample P2 and P5 (12% AF) which show relatively higher inclusion density (~6.05×10^4 no./mm^2) and relatively finer average inclusion size (0.157 μm and 0.172 μm) respectively. These results are close to the observations made by the previous investigators.[30,35–37]

The simple and cumulative size distribution of inclusion for samples P11 and P14 having maximum AF content (~36%) and for samples P2 and P5 having minimum AF content (12%) are shown in **Figs. 8** and **9** respectively. It is to be noted that a maximum amount of 36% AF which is considerably lower than the previous observations, has be achieved in the present study due to the lower frequency of inclusion (maxm. 14%) in the size range from 0.3 to 0.6 μm. The relatively coarser inclusions in samples P11, P14 and P15 compared to P2 and P5 could be associated with higher alloying elements such as Mn, Si, which can form oxide inclusions earlier and will get more time to

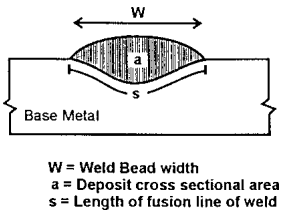

Fig. 10a. Reference for measurement of weld bead parameter: width (W), transverse cross sectional area (α) and fusion line length (s).

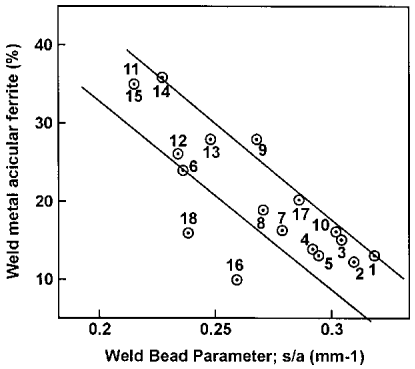

Fig. 10b. Variation of weld metal acicular ferrite content with weld bead parameter (s/a).

Fig. 11. TEM micro photograph of sample P14 showing acicular ferrite nucleated by inclusion within grain boundary.

grow. Tendency to coarsening of inclusions and transporting to the slag increases with the increase of alloying element, resulting in decrease of volume fraction of inclusions.[38]

The coarsening of inclusions may be also related to the weld pool solidification time. With the increase of weld pool solidification time, inclusions will get more time to grow.[38] Previous investigator[38] also reported that weld pool solidification time is inversely related to the weld bead parameter s/a. Where 's' is the length of fusion line of weld and 'a' is the transverse cross sectional area of the weld (**Fig. 10**(a)). Therefore, it is expected that, with the decrease of s/a value, weld pool solidification time increases with consequent increase of inclusion size, thus favouring the formation of AF in the weld metal microstructure. The increasing trend of AF content with the decrease of weld bead s/a value as observed in Fig. 10(b), supports such behaviour.

Since weld beads in the present set of experiments have been deposited at fixed welding parameters, the thermal conditions of the weld pool may be assumed to be remains same. Therefore, the change in s/a value of weld bead may be caused by variations in flux ingredients of experimental fluxes (Table 1), as flux ingredients has been also reported to affect the weld bead geometry.[38] Like AF and inclusion, the Prediction equation has been developed for weld bead parameter (s/a), in terms of flux ingredients as given below:

$$\begin{aligned}(s/a) = {} & 0.021494\mathrm{CaO} + 0.005513\mathrm{MgO} \\ & + 0.008605\mathrm{CaF_2} + 0.011134\mathrm{Al_2O_3} \\ & - 0.000402\mathrm{CaO \cdot MgO} \\ & - 0.000534\ \mathrm{CaO \cdot CaF_2} \\ & - 0.000666\mathrm{CaO \cdot Al_2O_3} \\ & - 0.000046\ \mathrm{MgO \cdot Al_2O_3} \\ & - 0.000093\ \mathrm{CaF_2 \cdot Al_2O_3} \quad \ldots\ldots\ldots\ldots\ldots\ldots (6)\end{aligned}$$

Similar to weld metal acicular ferrite content, inclusion volume fraction (V_f) and number density (D_o), the predominant effects of flux ingredients and their binary synergism/antagonism at 95% confidence level are also incorporated in Table 4. The details of regression models for s/a are also given in Appendix I.

The results of prediction of weld bead parameter (s/a) as given in Eq. (6) and Table 4 show that CaO increases s/a, impling that CaO acts in the way of decreasing inclusion size and hence does not favour AF formation. On the other hand, binary mixtures $CaO–CaF_2$ and $CaO–Al_2O_3$ decrease (binary antagonism) weld bead parameter (s/a) and hence act in the way of increasing inclusion size, thus favouring AF formation. This result is in complete agreement with the effect of CaO, $CaO–CaF_2$ and $CaO–Al_2O_3$ on AF content of weld metal as predicted in Eq. (3) and tabulated in Table 4.

The formation of AF by intragranular inclusion is evident in TEM photograph of sample P14 (**Fig. 11**). It is also worth to mention that higher amount of AF (36%) in sample P14 is also found to be associated with inclusions having higher amount of Al and lower amount of S as observed from the EDAX spectra on round shaped inclusion in sample P14 as shown in **Fig. 12**(a). Similar observation of AF formation associated with Al bearing inclusions not covered with sulphur coating have been reported by other investigators.[39,40] On the other hand, the irregular shaped inclusions with sulphur coating (Fig. 12(b)) as observed in sample P2 with lower value of acicular ferrite (12% AF) is found to be associated with lower amount of Al and higher amount of sulphur.

Although prior austenite grain size has an influence on AF formation as reported by previous investigates[35,37] measurement of prior austenite grain size for few selected samples in the present investigation as shown in **Table 6** indicate large scatter with no definite trend between AF content and prior austenite grain size.

6. Adequacy of the Developed Prediction Equation

The adequacy of the prediction equation developed by regression model for microstructural constituent acicular ferrite content was checked by performing submerged arc welding using randomly designed fluxes (**Table 7**). The experimentally determined and theoretically predicted results alongwith their residuals are given in **Table 8**. These results are compared graphically in **Fig. 13**. It is observed from Fig. 13 that there is reasonably good agreement between the experimental and predicted results. Therefore, the prediction model is quite adequate in describing weld metal microstructural constituent acicular ferrite.

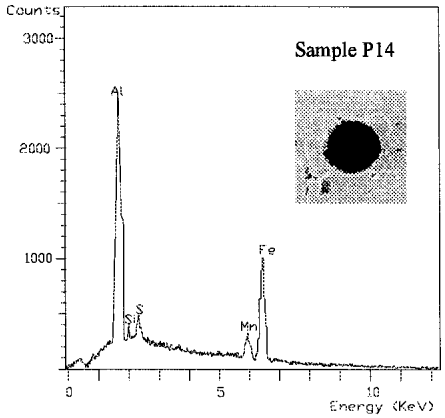

(a)

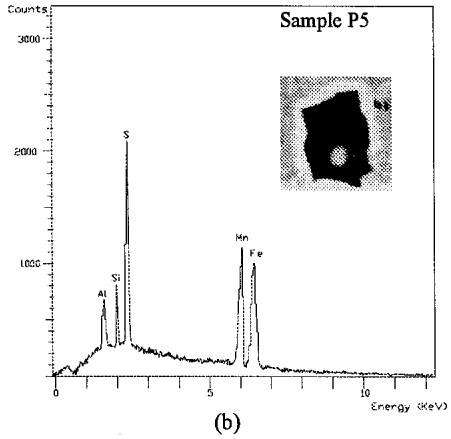

(b)

Fig. 12. EDAX spectra for inclusion located on weld metal (a) acicular ferrite, (b) grain boundary ferrite.

Table 6. Prior austenite grain size for selected weld metal sample.

Sample No.	Average Prior Austenite grain size (μm)
P4	70
P6	78
P14	75
P16	74
P17	80

Table 7. Randomly designed submerged arc flux composition.

Sample No.	Mixture Variables Composition			
	CaO (wt%)	MgO (wt%)	CaF_2 (wt%)	Al_2O_3 (wt%)
T1	17	20	30	13
T2	30	15	15	20
T3	25	30	15	10
T4	15	25	10	30
T5	20	28	12	20
T6	23	27	15	15
T7	19	18	11	32
T8	16	17	25	22

Other Additions to eighteen nos. of flux samples
Wt% SiO_2 = 10.0 Wt% Fe-Mn = 4.0
Wt% Bentonite = 2.0 Wt% Fe-Si = 3.0
Wt% Ni-Powder = 1.0

Table 8. Experimentally determined, predicted and residuals of weld metal acicular ferrite content obtained in experiments using randomly designde flux.

Sample No.	Acicular ferrite Experimentally obtained (%)	Acicular ferrite Predicted from Equation 3 (%)	Residual (%)
T1	15.4	16.6	1.2
T2	31.3	32.7	1.4
T3	32.5	31.0	1.5
T4	11.0	9.0	2.0
T5	24.7	24.5	0.2
T6	29.8	28.0	1.8
T7	20.8	22.9	2.1
T8	15.2	14.4	0.8

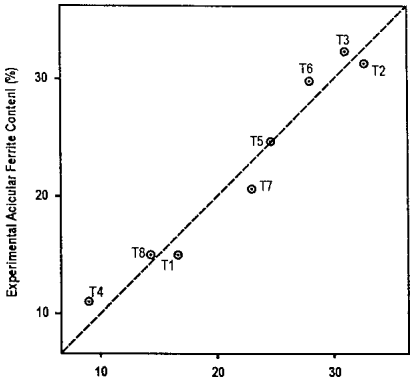

Fig. 13. Comparison between experimental and predicted results for weld metal acicular ferrite content.

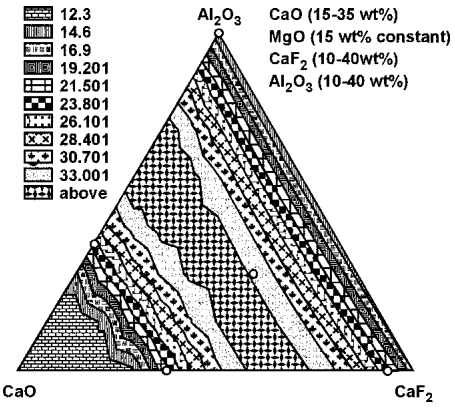

Fig. 14. I so-response contour plots for Weld metal acicular ferrite content at different flux composition.

The iso-response contour plots for acicular ferrite content is also developed as shown in **Fig. 14**. The shades in the figure represent the value of acicular ferrite content which can be obtained at different combination of flux ingredients *viz*. CaO, CaF_2 and Al_2O_3 at fixed MgO content (15% minimum) in the present experiment. This has been done because, these three ingredients (CaO, CaF_2, Al_2O_3) reported to have predominant effect on weld metal acicular ferrite content.

7. Conclusion

Following conclusions can be drawn from the present

study.

(1) The submerged arc weld metal microstructural constituent acicular ferrite may be predicted in terms of flux ingredients by developing regression equations, with the help of statistical experiments for mixture design.

(2) The binary mixtures of CaO *viz*. CaO–CaF_2 and CaO–Al_2O_3 have binary synergistic (increasing) effect on weld metal acicular ferrite content.

(3) Flux ingredient CaO decreases acicular ferrite content, but other ingredient MgO has not any predominant effect on acicular ferrite content.

(4) Flux mixtures CaO–CaF_2 and CaO–Al_2O_3 increases (binary synergism) acicular ferrite content by controlling both chemical composition and inclusion characteristics of weld metal.

(5) CaO–MgO, MgO–CaF_2, MgO–Al_2O_3 and CaF_2–Al_2O_3 retard acicular ferrite formation by forming more number of inclusions.

(6) Flux ingredients also have an influence on acicular ferrite formation by changing weld pool solidification time through weld bead parameter (*s*/*a*).

REFERENCES

1) O. Grong and D. K. Matlock: *Int. Met. Rev.*, **31** (1986), 27.
2) A. G. Glover, J. T. McGrath, M. J. Trukler and G. C. Weatherly: *Weld. J.*, **56** (1977), 267.
3) D. W. Oh, D. L. Olson and R. H. Frost: Welding and Joining Processes, PED–5A, ed. by E. Hannatey-Asibu, Jr., H. S. Cho and S. Fukuda, ASME, New York, (1991), 49.
4) R. C. Cochrane, J. L. Ward and B. R. Keville: Proc. of the Int. Conf. on the Effects of Residual, Impurity and Micro Alloying Elements on Weldability and Weld Properties, The Welding Institute, London, (1983), Paper 16.
5) G. S. Barritte and D. V. Edmonds: Proc. Conf. on Advances in the Physical Metallurgy of Steel, The Metals Society, London, (1981), 126.
6) D. J. Abson, R. E. Dolby and R. H. Hart: Proc. Int. Conf. on Trends in Steel and Consumables for Welding, The Welding Institute, London, (1978), 75.
7) T. H. North, H. B. Bell, A. Koukabi and I. Craig: *Weld. J.*, **58** (1979), 343.
8) R. A. Ricks, P. R. Howell and G. J. Barrite: *J. Mater. Sci.*, **17** (1983), 732.
9) E. S. Kayali, J. M. Corbett and H. W. Kerr: *J. Mater. Sci. Lett.*, **2** (1983), 123.
10) H. K. D. H. Bhadesia: Bainite in Steels, The Institute of Metals, London, (1992), 309.
11) G. R. Edwards and S. Liu: Proc. of the First United States—Japan Symp. on Advances in Welding Metallurgy, American Welding Society, Japanese Welding Society, Japanese Welding Engineering Society, Sanfrancisco, California, US and Yokohama, (1990), 218.
12) O. Grong and D. K. Matlock: *Int. Met. Rev.*, **31** (1986), 27.
13) C. B. Dallam, S. Liu and D. L. Olson: *Weld. J.*, **64** (1985), 140.
14) S. S. Babu, S. A. David, J. M. Vitek, K. Kundra and T. Deb Roy: *MST*, **11** (1995), 186.
15) M. L. E. Davis and N. Bailey: Proc Int. Conf. on Trends in Steels and Consumables for Welding, London, The Welding Institute, London, (1980), Paper 34, 289.
16) T. W. Eagar: *Weld. J.*, **57** (1978), 76.
17) M. L. E. Davis and N. Bailey: Proc. Int. Conf. on Trends in Steels and Consumables for Welding, The Welding Institute, London, Paper 34, (1980), 289.
18) T. Lau, G. C. Weatherly and A. Molem: *Weld. J.*, **12** (1985), 343.
19) M. A. B. Moor, T. H. North and H. B. Bell: *Weld. Met. Fabr.*, (1978), 193.
20) M. L. E. Davis and F. R. Coe: The Welding Institute Research Report, No. 39/1977/M, (1977), 1.
21) C. S. Chai and T.W. Eagar: *Weld. J.*, **61** (1982), 229.
22) A. Polar, J. E. Indacochea and M. Blander: *Weld. J.*, **70** (1991), 15.
23) M. L. E. Davis and N. Bailey: Proc. of the Int. Conf. on trends in Steels and Consumables for Welding, Paper 19, The Welding Institute, London, (1978), 231.
24) R. A. Mclean and V. L. Anderson: *Technometrics*, **8** (1966), 447.
25) R. D. Snee and D. W. Marquardt: *Technometrics*, **18** (1976), 19.
26) R. D. Snee and D. W. Marquardt: *Technometrics*, **16** (1974), 399.
27) R. D. Snee: *Communications in Statistics*; *Theory and Method*s, **48** (1979), No. 4. 303.
28) J. Jang and J.E. Indacochea,: *JOMS*, **22** (1987), 689.
29) C. W. Ramsay, D. K. Matlock and D. L. Olson: Proc. of the 2nd Int. Conf. on Trends in Welding Research, ASM International, Ohio, (1989), 763.
30) R. A. Farrar and P. L. Harrison: *JOMS*, **22** (1987), 3812.
31) S. Liu, D. L. Olson, S. Ibarra and O. Runnerstam: Proc. of the Twenty Firth Annual Technical Meeting of the Int. Metallographic Society, 20 (1993), 31.
32) R. A. Farrar and M. N. Watson: *Met. Constr.*, **11** (1979), 285.
33) P. Kanjilal, T. K. Pal and S. K. Majumdar: *Scand. J. Metall.*, **33** (2004), June, 146.
34) S. Ibarra, D. L. Olson and S. Liu, Proc. of the Ninth Int. Conf. & Offshose Mechanics and Arctic Engineering, ASME, New York, (1990), 517.
35) S. Liu and D. L. Olson: *Weld. J.*, **65** (1986), June, 139.
36) D. J. Abson, R. E. Dolby and P. H. M. Hart: Proc. Int. Conf. on Trends in Steel and Consumables for Welding, The Welding Institute, London, (1978), Paper 25, 75.
37) O. Grong and D. K. Matlock: *Int. Met. Rev.*, **31** (1986), No. 1, 27.
38) U. Mitra and T. W. Eagar: *Metall. Trans. B*, **22B** (1991), 83.
39) L. Devillers, D. Kaplan, B. Marandet, A. Ribes and P. V. Riboud: Proc. Int. Conf. on the Effects of Residual Impurity and Microalloying Element on Weldability and Weld Properties, The Welding Institute, London, (1983), 1.
40) D. J. Abson: Welding in the World, 1989, Vol. 27 (3/4) IIW, Doc. IX–1486–87, May, (1987), 1.

Appendix I. '*t*' value and significant level (P) of each predictor for the responses of weld metal acicular ferrite (AF) inclusion volume fraction (V_f) inclusion no. density (D_o) and weld bead parameter (*s*/*a*).

Predictors	Responses				Responses			
	AF		s/a		V_f		D_o	
	t	Sig. (P)	t	Sig. (P)	t	Sig. (P)	t	Sig. (P)
CaO	–3.08271	.015055	3.50280	.008046	0.527072	0.612442	0.18835	0.855292
MgO	.96180	.364316	.65111	.533227	0.620704	0.552064	-1.00905	0.342491
CaF_2	–.57635	.580228	3.44342	.008779	2.498053	0.037054	1.28409	0.235048
Al_2O_3	–.86055	.414530	3.56522	.007345	1.333912	0.218957	0.68377	0.513435
CaO-MgO	1.17597	.273413	–1.59610	.149134	0.963401	0.363560	3.18328	0.012934
CaO-CaF_2	3.39172	.009476	–2.98197	.017548	0.764191	0.466692	1.99005	0.081766
CaO-Al_2O_3	3.41523	.009152	–3.41407	.009168	0.346114	0.738184	2.47713	0.038283
MgO-CaF_2	–1.24702	.247660	–.19875	.847416	1.034465	0.331174	1.66186	0.135117
MgO-Al_2O_3	–1.15819	.280191	–.02847	.977984	0.282226	0.784934	2.30976	0.049707
CaF_2-Al_2O_3	–.16375	.873986	–.57552	.580764	1.109819	0.299320	2.74417	0.025286

ANOVA of Responses

Response	Regression Details	Sum of Squares (SS)	df	Mean Sum of Square (MS)	F	P
AF	Model Residual	861.339 382.439	9 8	95.70432 47.80486	2.001979	0.170642
s/a	Model Residual	.013103 .005857	9 8	.001456 .000732	1.988543	0.172970
Vf	Model Residual	113.0068 129.2710	9 8	12.55631 16.15887	0.777053	0.644506
Do	Model Residual	290.8952 55.38261	9 8	32.32169 6.922826	4.668857	0.020453

Appendix II.[33)]

$$\text{Oxygen}(O_2\,\text{ppm}) = 63.305CaO - 12.420MgO + 6.457CaF_2 + 16.775Al_2O_3 - 0.945CaO\cdot MgO - 1.557CaO\cdot CaF_2 - 2.061CaO\cdot Al_2O_3 + 0.835MgO\cdot CaF_2 + 0.767MgO\cdot Al_2O_3 + 0.378CaF_2\cdot Al_2O_3 \quad (1)$$

$$\text{Manganese}(Mn\%) = .0244CaO + .0590MgO + .0012CaF_2 + .0024Al_2O_3 - .0004CaO\cdot MgO + .0012CaO\cdot CaF_2 + .0013CaO\cdot Al_2O_3 - .0013MgO\cdot CaF_2 + .0014MgO\cdot Al_2O_3 + .0002CaF_2\cdot Al_2O_3 \quad (2)$$

$$\text{Silicon}(Si\%) = .0107CaO + .0520MgO + .0083CaF_2 + .0128Al_2O_3 - .0011CaO\cdot MgO - .0001CaO\cdot CaF_2 - .00008CaO\cdot Al_2O_3 - .0012MgO\cdot CaF_2 - .0013MgO\cdot Al_2O_3 + .0002CaF_2\cdot Al_2O_3 \quad (3)$$

$$\text{Sulphur}(S\%) = .00312CaO + .00471MgO + .00181CaF_2 + .00220Al_2O_3 - .00015CaO\cdot MgO - .00007CaO\cdot CaF_2 - .00008CaO\cdot Al_2O_3 - .0009MgO\cdot CaF_2 - .00011MgO\cdot Al_2O_3 - .00002CaF_2 \quad (4)$$

$$\text{Nickel}(Ni\%) = -.0776CaO + .0556MgO - .0181CaF_2 - .0058Al_2O_3 + .0006CaO\cdot MgO + .0030CaO\cdot CaF_2 + .0026CaO\cdot Al_2O_3 - .0015MgO\cdot CaF_2 - .0018MgO\cdot Al_2O_3 + .0004CaF_2\cdot Al_2O_3 \quad (5)$$

$$\text{Carbon}(C\%) = -.00118CaO + .00656MgO + .00185CaF_2 - .00034Al_2O_3 - .00009CaO\cdot MgO + .00007CaO\cdot CaF_2 + .00017CaO\cdot Al_2O_3 - .00016MgO\cdot CaF_2 - .00013MgO\cdot Al_2O_3 - .00002CaF_2\cdot Al_2O_3 \quad (6)$$

Table A1. Predominant effect of flux ingredients and their binary mixtures on weld metal chemical composition.

(Response characteristics) Weld Metal Chemical constituents	Predominant Effects			
	Pure flux Ingredient		Binary Mixtures of Flux Ingredient	
	Increase	Decrease	Synergism	Antagonism
Oxygen	CaO, CaF_2, Al_2O_3	—	MgO-CaF_2 MgO-Al_2O_3 CaF_2-Al_2O_3	CaO-MgO CaO-CaF_2, CaO-Al_2O_3
Mangaese	MgO	CaO	CaO-CaF_2, CaO-Al_2O_3	MgO-CaF_2 MgO-Al_2O_3
Silicon	CaO, MgO, CaF_2, Al_2O_3	—	—	CaO-MgO, MgO-CaF_2 MgO-Al_2O_3
Sulphur	CaO, MgO, CaF_2, Al_2O_3	—	—	CaO-MgO, CaO-CaF_2, CaO-Al_2O_3 MgO-CaF_2 MgO-Al_2O_3
Nickel	MgO	CaO, CaF_2,	CaO-CaF_2, CaO-Al_2O_3	MgO-CaF_2 MgO-Al_2O_3
Carbon	MgO-CaF_2	—	CaO-CaF_2, CaO-Al_2O_3	CaO-MgO, MgO-CaF_2 MgO-Al_2O_3